Supplement of Atmos. Chem. Phys., 24, 1873–1893, 2024
https://doi.org/10.5194/acp-24-1873-2024-supplement
© Author(s) 2024. CC BY 4.0 License.

Atmospheric Chemistry and Physics
Open Access
EGU

Supplement of

Iodine oxoacids and their roles in sub-3 nm particle growth in polluted urban environments

Ying Zhang et al.

Correspondence to: Xu-Cheng He (xucheng.he@helsinki.fi) and Wei Nie (niewei@nju.edu.cn)

The copyright of individual parts of the supplement might differ from the article licence.

Text

S1. Field measurements of sulphur dioxide (SO_2) at two sites

SO_2 is measured continuously at the SORPES station using a Thermo TEI 43i. At BUCT/AHL station, SO_2 is measured with the same analyser. Due to an instrument malfunction, SO_2 concentration is discarded in October and November, 2020 at the BUCT/AHL station. The long-term time traces of daytime (08:00~16:00 LT) mean SO_2 and its seasonal and monthly variations at both sites are depicted in Fig. S12. SO_2 is primarily emitted through coal combustion in heating seasons in Beijing. The official onset of the heating period in Beijing is 15th November and the heating ends on 15th March the following year. The SO_2 at BUCT/AHL site is strongly enhanced by the release of SO_2 in heating seasons (grey shade area). It is worth noting that the measured concentrations of SO_2 at the BUCT/AHL station is higher than that of the SORPES station in winter (January and February), which could partially explain the higher concentration of H_2SO_4 measured in Beijing.

S2. Classification of growth time span at SORPES

A Neutral cluster and Air Ion Spectrometer (NAIS, Airel Ltd., Estonia) (Manninen et al., 2016) was deployed to detect the particle number size distribution (PNSD) in the early stages of NPF at the SORPES station. The negatively charged particles in the size range of around 0.8 nm to 42 nm were measured to study the growth of newly formed particles. However, the limited charges are likely to be captured by larger particles in polluted urban environments which leaves it difficult for us to track the growth trajectory of sub-3 nm particles in NPF events in the SORPES station.

To compare the contribution of gaseous HIO_3 in the subsequent growth of newly formed particles in NPF events at the SORPES station, we further developed a new method by considering gaseous H_2SO_4 as the governing GR contributor as mentioned in 2.2.2. To get the average acid concentration, the general NPF timespan needs to be determined. Though the growth trajectories of smaller particles are vague in this study, the 50% appearance time at approximately 7 nm, where the PNSD shows a sharp increase, can be identified (Kulmala et al., 2012). The 50% appearance time at 7 nm is therefore regarded as the end time

for the particle formation as this study focuses on the sub-7 nm particle growth processes. We further find the start time of NPF events by extrapolating different hours backward in time. To better reflect the uncertainty induced by different timespans, we further show the statistical results for each timespan in Fig. S11. As the acid concentration time resolution is 30 min, different time spans (0.5, 1, 1.5 and 2 hours) are investigated to determine which one is the most suitable for all individual NPF cases. Fig. S11(a) shows the scatterplot of iodic acid contribution to growth versus that of sulfuric acid for sub-3 nm particles. The GR contribution of IA accounts for no less than 1% and no larger than 20% compared to SA. It should be noted that the slope of the fitted line remains nearly unchanged and the ratio varies inconspicuously as the timespan increases from 0.5 h to 2 h. Therefore, different timespan determination will not induce significant uncertainty in the calculated GR contribution. Fig. S11(b) shows the boxplot of the ratio of iodic acid contribution to that of sulfuric acid for sub-3 nm particles using different timespans. It can be seen that with the increasement of growth timespan from 0.5 h to 2 h, the contribution ratio rise insignificantly. We therefore choose the 2 hours timespan in this study as the sub-7 nm growth in Beijing is regularly at a few nanometers per hour (Table S2 – S9) and a 2-hours window should generally contain the period when the particles grow from sub-3 nm to 7 nm. The statistical result for all NPF events at the SORPES station is depicted in Fig. S11(c).

S3. The sensitivity of survival probability

The non-linear relationship between survival probability and growth rate and the coagulation sink given by Eq. (8) suggests that a small perturbation of growth rate could lead to a significant shift of particle survival probability. As depicted in Fig. 5, the theoretical SP for both sub-3 nm and 3-7 nm particles can vary significantly with different coagulation sink and growth rates. At a fixed coagulation sink, the difference in GR of a factor of 10 contributes to a difference in SP of a factor of around 1000, which reflects that the SP of particles are extremely sensitive to the change of GR.

To further illustrate this sensitivity of survival probability to growth rate change, we quantify the sensitivity of SP to particle GR difference (ΔGR) in Fig. S13. The sensitivity of SP in this study is quantified using the amplification of SP induced by GR difference (X-axis) and is calculated according to

$$\text{SP amplification} = \frac{\text{SP}(\text{GR}_0 + \Delta\text{GR})}{\text{SP}(\text{GR}_0)} \quad \text{(S1)}$$

where GR_0 refers to the initial growth rate of particles, and ΔGR is the difference in GR. $\text{SP}(GR_0)$ and $\text{SP}(\text{GR}_0 + \Delta\text{GR})$ are the theoretical SP calculated using Eq. (8). The results of SP amplification with different GR_0 (1.0 and 1.5 nm h^{-1}) are shown in Fig. S13(b) and S13(c), respectively. The amplification of SP caused by additional GR enhancement is both subject to the particle diameter, d_p and GR_0. Fig. S13(b) shows that for particles growing initially at the rate of 1.0 nm h^{-1}, the smaller the particles are and the larger the GR increases, the more significant the amplification of SP. Fig. S13(c) depicts that particle SP will be amplified less significantly if particles grow at a higher initial rate (1.5 nm h^{-1}). To better bridge the gap between measurement results and theoretical calculation, Fig. S13(a) shows the frequency distribution of iodic acid GR contribution at the SORPES station as a case study. At the SORPES station, sulphuric acid dominates the initial growth of sub-3 nm particles. Therefore, GR contribution of IA can be taken into consideration as additional GR increment (ΔGR). For new particles growing at the rate of around 1 nm h^{-1} at the SORPES station, iodic acid as an additional GR contributor could regularly amplify the particles SP to 2 orders of magnitude higher. Fig. S11(c) also illustrate that iodic acid GR contribution will significantly enhance the SP of sub-3 nm particles accounting for no more than 20% of sulphuric acid GR contribution. This case study shows that the high sensitivity of particles SP to GR difference makes it rather difficult to characterize an NPF event, especially in urban environments with various GR contributors.

S4. Cluster analysis of backward trajectories

To analyse the air masses reaching the AHL/BUCT site, we conducted cluster analysis of backward trajectory using the TrajStat model, a plug-in of MeteoInfo software (Wang, 2014). The calculation of trajectories was based on the Hybrid Single-Particle Lagrangian Integrated Trajectory (HYSPLIT) model (Stein et al., 2015). As depicted in Fig. S5, the 3-day backward trajectories at 500 m above the ground level of the AHL/BUCT station (39˚56′N, 116˚17′E) are clustered by examining the total spatial variance (TSV).

S5. The calculation method of GRs in NPF events

The growth of newly formed particles for NPF events are often reflected by the collective shift of measured particle size distribution towards larger sizes as time evolves, and it is unfeasible to track the growth of a single particle based on the measurements. Therefore, both approaches used in this study (mode-fitting and appearance time) are referred to as collective approaches and the GRs in this study are the estimated ones (Stolzenburg et al., 2023). While using mode-fitting method, the growth trajectory of new particles is represented by the peak diameter (d_p) of the nucleation mode, which is determined after applying log-normal distributions to the measured size distribution (Kulmala et al., 2012). For measured particle number size distribution at each time (t), there will be a d_p, and the value of GR (GR_{mode}) is derived by a linear fit to the d_p vs t.

Instead of tracking the shift of peak diameter for a given time period, appearance time method seeks to find the time it takes (Δt) for the particle to grow between instrument size bins (Δd_p). In this study, we take the time (t) that the measured concentration of particles reaches its half maximum for each d_p. For each particle size bin (d_p) of the instrument used at BUCT/AHL, there will be a t, and the value of GR (GR_{apt}) is derived by a linear fit to the d_p vs t. Additionally, we believe it would be conceptually more correct to consider diameter as the independent variable when fitting the GRs using appearance time method although previous studies commonly take appearance time as the independent variable and diameter as the dependent variable when fitting the GRs. that is because each data point corresponds to a precise size bin, and any variation (largely stemming from uncertainty due to atmospheric heterogeneity) among the data points primarily exists in appearance time. Consequently, the fitting method with diameter as the independent variable was named as APT-y and the one with time as the independent variable was called as APT-x.

Figures

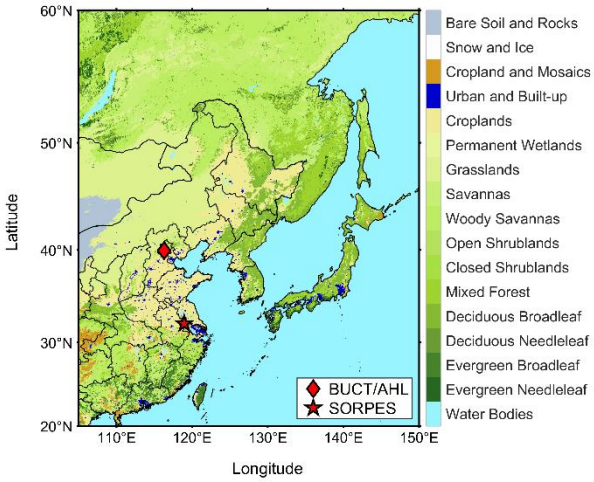

Figure S1. The geophysical distribution of two measurement sites (BUCT/AHL in Beijing, China and SORPES in Nanjing, China) of this study. The types of land cover were obtained from the Terra and Aqua combined Moderate Resolution Imaging Spectroradiometer (MODIS) Land Cover Type (MCD12Q1) (https://lpdaac.usgs.gov/products/mcd12q1v006/, last access: 11 November 2023).

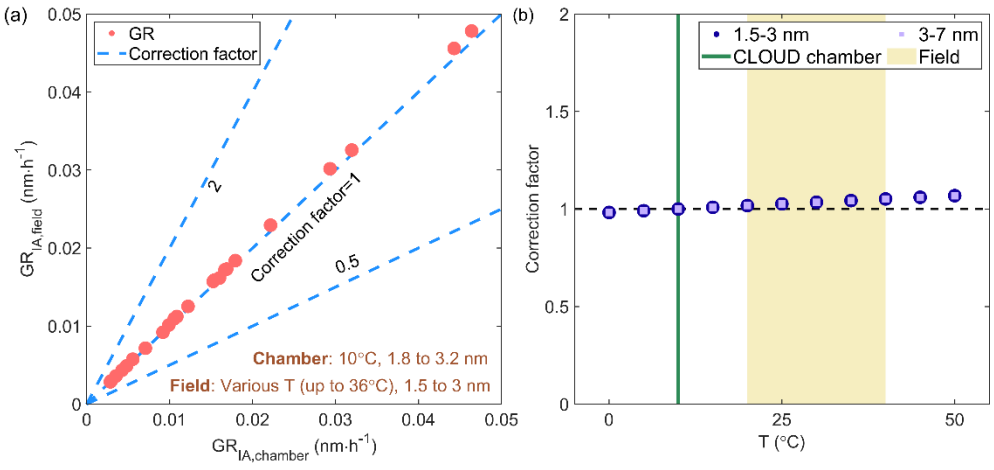

Figure S2. The calculated correction factors based on Eq. (10) and the sensitivity against temperature and size. (a) The correction factors derived based on chamber and field site measurement conditions during NPF events. (b) The correction factor as a function of temperature with different points denoting the selected size ranges.

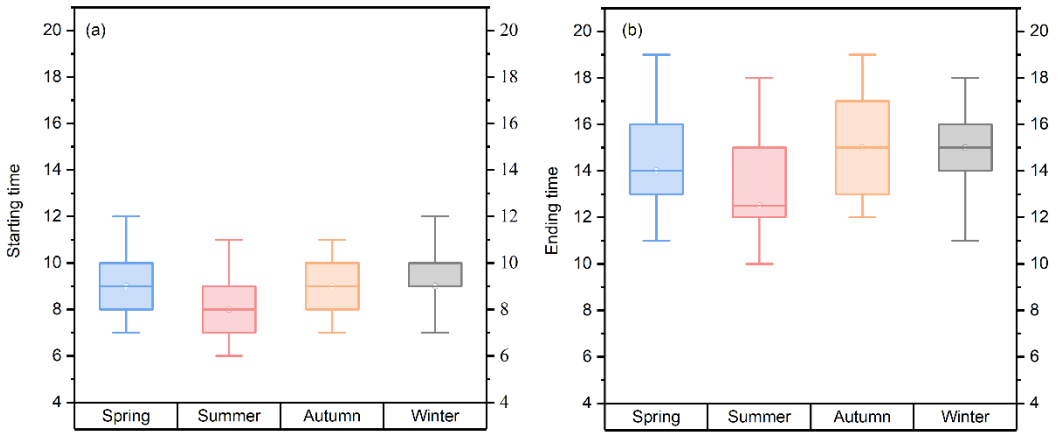

Figure S3. Starting time (a) and ending time (b) of NPF events in Beijing four seasons.

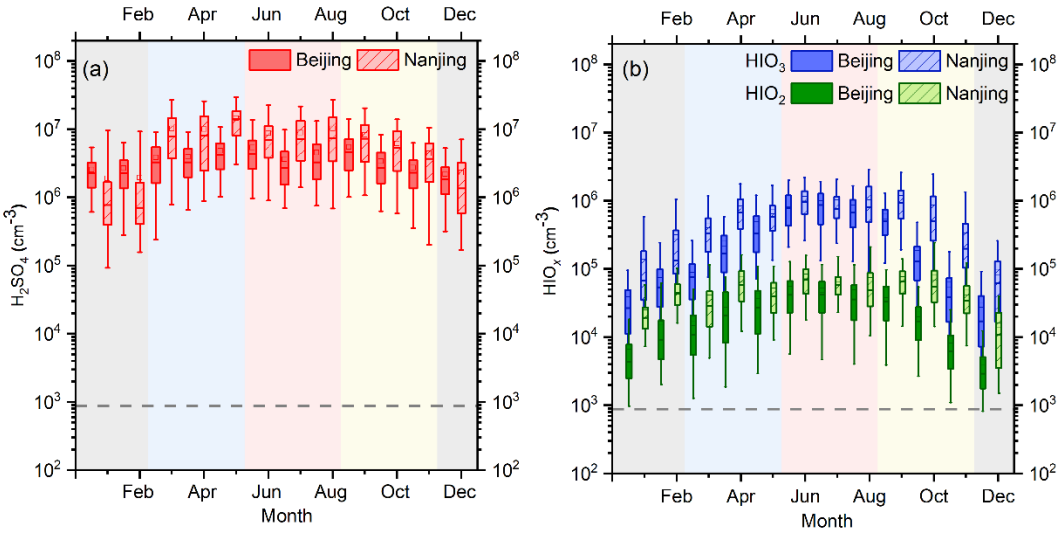

Figure S4. Monthly variation of sulfuric acid and iodine oxoacid concentrations in Beijing and Nanjing.

125

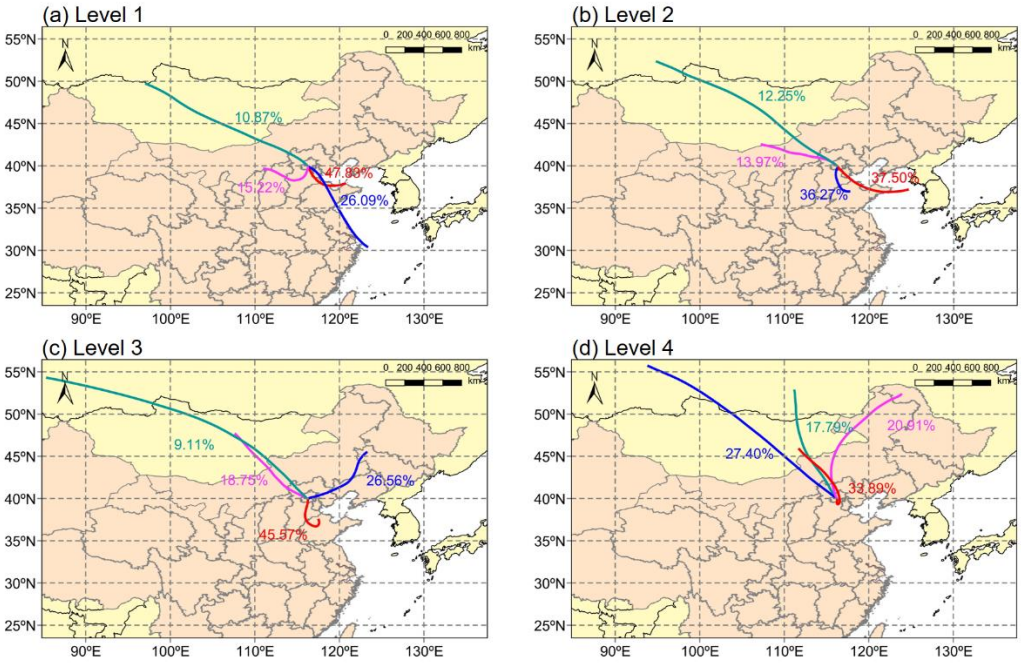

Figure S5. The cluster analysis in different HIO_3 precursors intensities. The four levels of the proxy concentration of HIO_3 precursors are in the 75% - 100%, 50%-75%, 25%-50%, 0-25% percentiles from the first to the fourth levels, respectively. The percentage of each trajectory reflects the ratio of the corresponding cluster.

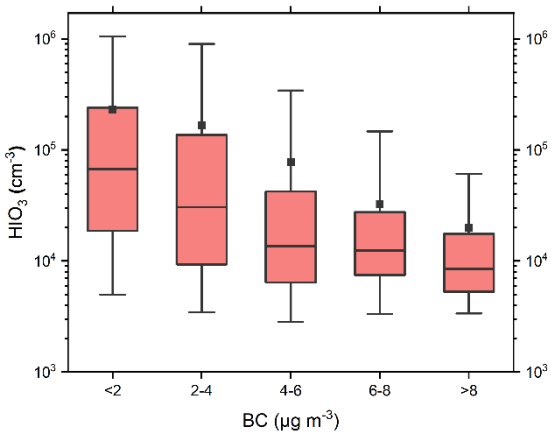

130

Figure S6. HIO_3 concentration in different BC level bins.

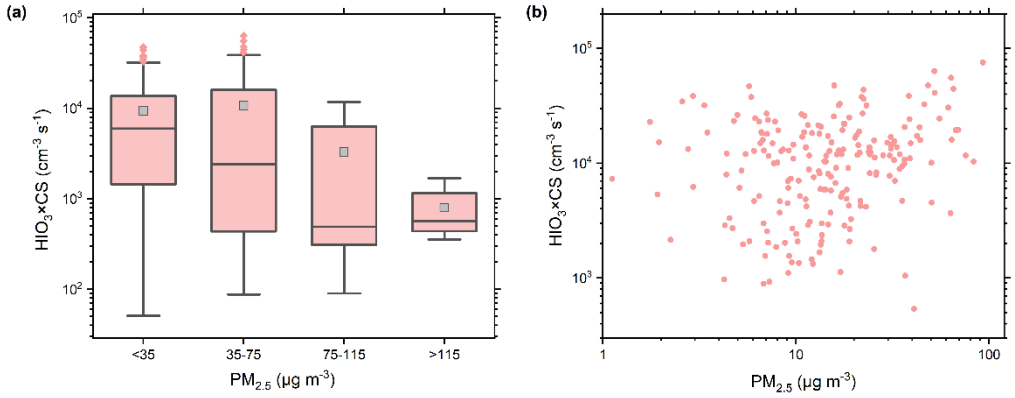

Figure S7. The impact of $PM_{2.5}$ on HIO_3 production calculated from the HIO_3 concentration and CS (a) in all seasons and (b) specifically in warm seasons (from May to September).

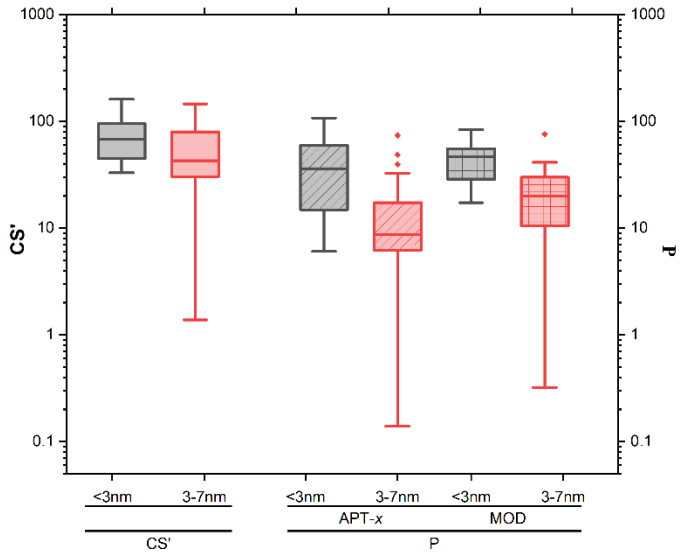

Figure S8. The dimensionless CS' and P in the growth periods within sub-3 nm and 3-7 nm in Beijing. Here, CS' are calculated from CS (unit: s^{-1}) divided by 10^{-4} s^{-1} and the P is the ratio of CS' and GR' (GR/(1 nm h^{-1})). Both of them are calculated based on Kulmala et al. (2017).

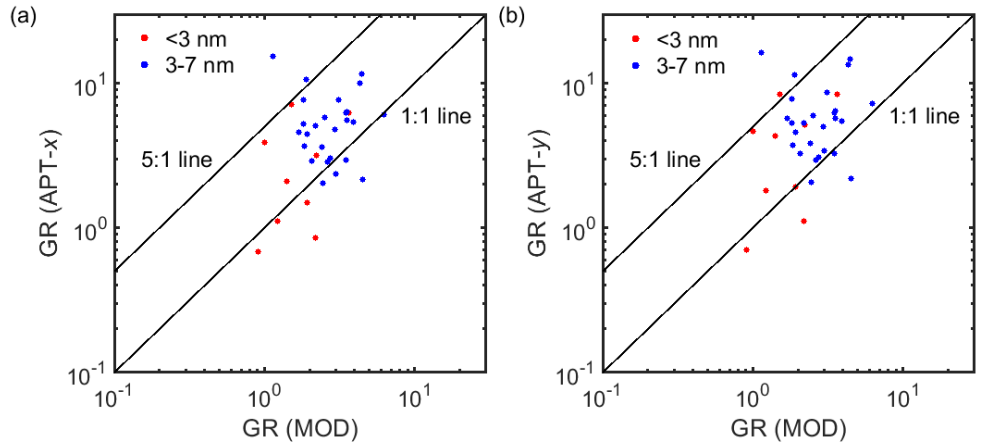

Figure S9. The measured GR comparison between two different methods. (a) Comparison between APT-*x* and MOD and (b) comparison between APT-*y* and MOD.

145

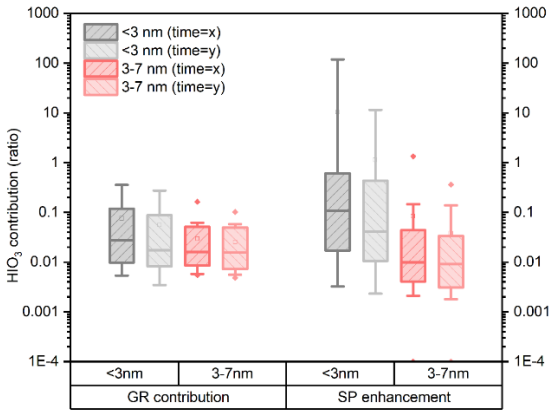

Figure S10. The contributions of HIO_3 to growth rate and survival probability of particles within sub-3nm and 3-7 nm in NPF events using the 50% appearance time method.

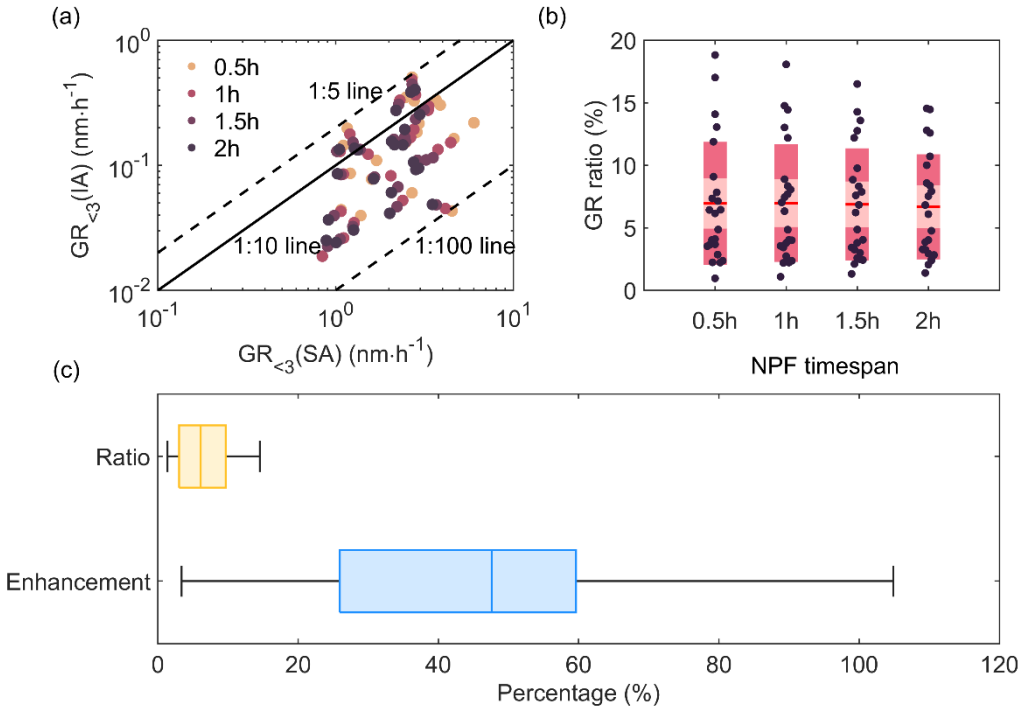

Figure S11. Determination of NPF timespan and the statistical result showing the GR contribution and hence SP enhancement in percentage considering HIO_3 as additional GR contributor. The scatterplot of GR contribution of HIO_3 to particles growing from 1.5 nm to 3nm versus that of H_2SO_4 coloured by different NPF timespans is presented in (a). Boxplots of the calculated ratio are shown in (b), in which the red solid line in the middle is the mean value of contribution ratio in each timespan bin. Calculted GR ratio for each NPF events are points drawn along Y axis. Points are laid over a 1.96 SEM (95% confidence interval) area shaded in rosy brown and one standard deviation area shaded in dark red. The boxplots for GR contribution ratio and SP enhancements at the SORPES station are depicted in (c).

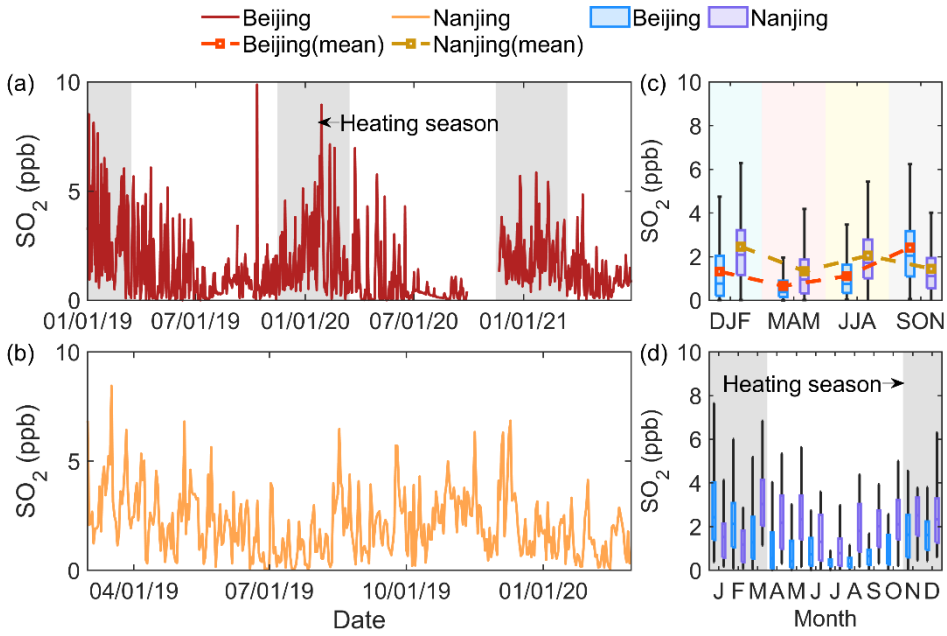

160

Figure S12. Measurements of SO_2 at two sites. The time traces of measured mean values of daytime (08:00~16:00 LT) SO_2 are shown in (a) and (b) for the BUCT/AHL station and the SORPES station, respectively. Seasonal (c) and monthly (d) variations at both sites are computed by the daytime mean values as well. The heating period in Beijing are depicted by the grey shaded areas in (a) and (c).

165

170

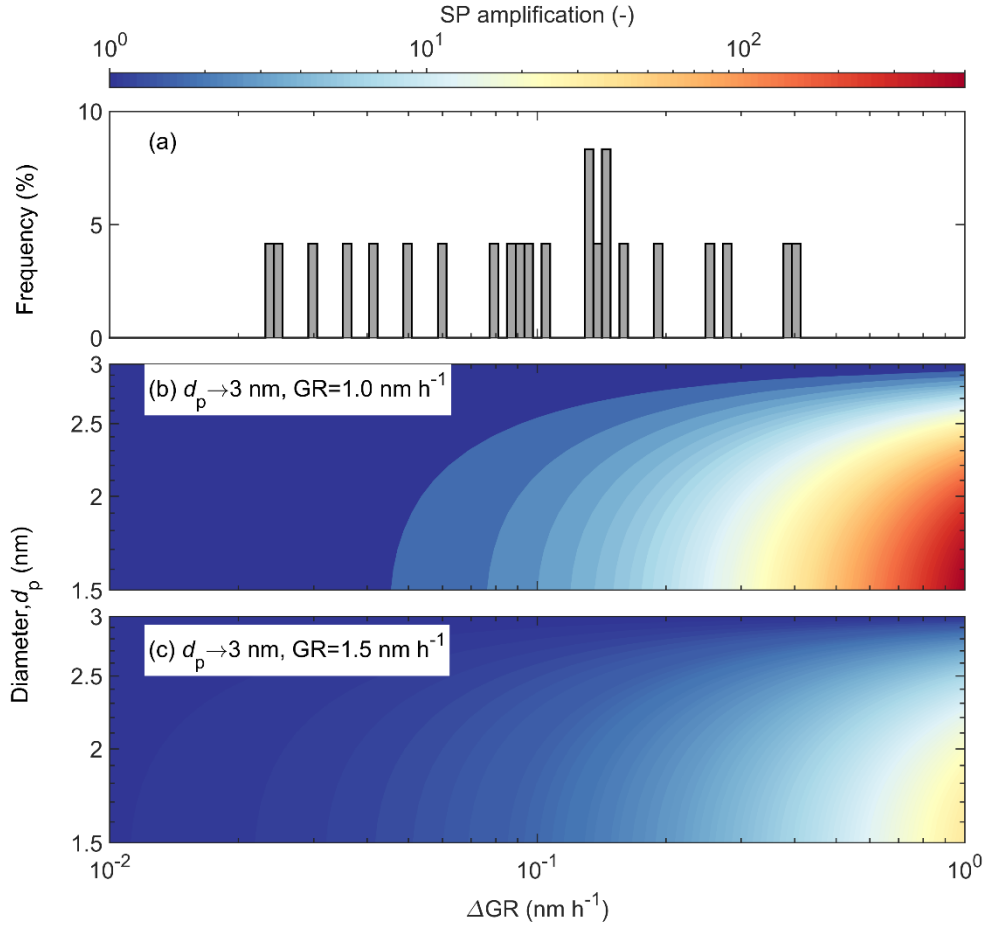

Figure S13. Amplification of survival probability under different GR enhancements and initial diameters. The amplification of SP is defined as the ratio of SP calculated with and without additional GR. (a)The frequency distribution of GR contribution of IA to sub-3 nm particle growth at the SORPES. (b) The amplification factor distribution of particles growing up to 3 nm with initial GR equals to 1.0 nm/h. (c) The amplification factor distribution of particles growing up to 3 nm with initial GR equals to 1.5 nm/h.

Tables

Table S1. NPF frequencies at both sites.

DATE	Beijing				Nanjing			
	NPFs (A+B)	non-NPFs	valid days	frequency	NPFs (A+B)	non-NPFs	valid days	frequency
2019-01	8 (7+1)	13	21	38.1%	-*	-	-	-
2019-02	8 (7+1)	20	28	28.6%	-	-	-	-
2019-03	14 (10+4)	15	29	48.3%	20 (5+15)	11	31	64.5%
2019-04	12 (6+6)	17	29	41.4%	12 (7+5)	18	30	40.0%
2019-05	12 (8+4)	17	29	41.4%	22 (15+7)	9	31	71.0%
2019-06	5 (2+3)	19	24	20.8%	16 (2+14)	14	30	53.3%
2019-07	4 (2+2)	26	30	13.3%	17 (5+12)	12	29	58.6%
2019-08	11 (7+4)	20	31	35.5%	21 (5+16)	10	31	67.7%
2019-09	9 (3+6)	21	30	30.0%	4 (0+4)	6	10	40.0%
2019-10	8 (7+1)	19	27	29.6%	11 (4+7)	3	14	78.6%
2019-11	3 (3+0)	16	19	15.8%	12 (7+5)	13	25	48.0%
2019-12	9 (7+2)	19	28	32.1%	8 (1+7)	17	25	32.0%
2020-01	5 (4+1)	13	18	27.8%	7 (2+5)	23	30	23.3%
2020-02	5 (3+2)	20	25	20.0%	10 (2+8)	19	29	34.5%
2020-03	13 (11+2)	18	31	41.9%	-	-	-	-
2020-04	12 (10+2)	16	28	42.9%	-	-	-	-
2020-05	9 (5+4)	17	26	34.6%	-	-	-	-
2020-06	6 (3+3)	23	29	20.7%	-	-	-	-
2020-07	0 (0+0)	26	26	0.0%	-	-	-	-
2020-08	1 (0+1)	12	13	7.7%	-	-	-	-
2020-09	7 (3+4)	10	17	41.2%	-	-	-	-
2020-10	12 (9+3)	17	29	41.4%	-	-	-	-
2020-11	8 (6+2)	19	27	29.6%	-	-	-	-
2020-12	7 (6+1)	15	22	31.8%	-	-	-	-

DATE	Beijing				Nanjing			
	NPFs (A+B)	non-NPFs	valid days	frequency	NPFs (A+B)	non-NPFs	valid days	frequency
2021-01	7 (3+4)	16	23	30.4%	-	-	-	-
2021-02	6 (3+3)	13	19	31.6%	-	-	-	-
2021-03	10 (5+5)	17	27	37.0%	-	-	-	-
2021-04	6 (4+2)	19	25	24.0%	-	-	-	-
2021-05	11 (9+2)	17	28	39.3%	-	-	-	-
2021-06	6 (4+2)	19	25	24.0%	-	-	-	-
2021-07	0 (0+0)	24	24	0.0%	-	-	-	-
2021-08	4 (2+2)	20	24	16.7%	-	-	-	-
2021-09	2 (1+1)	22	24	8.3%	-	-	-	-
2021-10	9 (5+4)	14	23	39.1%				
Total	249	609	858	29.0%	160	155	315	50.8%

Note: * represents the missing data.

Table S2. The GR contributions and SP enhancements of HIO_3 to particles in the size range between 1.5 nm to 3 nm on each NPF event days in Beijing based on APT-x.

Date	$CoagS_{1.5}$	$GR_{<3}$	GR_{H2SO4}	P1*	$GR_{<3}$ - GR_{HIO3}	P2*	GR contribution	$SP_{1.5-3}$ EF
20190818	2.21E-03	1.11	1.38	2.64E-03	1.07	2.16E-03	3.3%	22.2%
20190823	3.13E-03	3.01	1.63	4.57E-02	2.99	4.49E-02	0.5%	1.7%
20190830	1.91E-03	6.22	1.26	4.01E-01	6.17	3.99E-01	0.7%	0.7%
20210525	1.40E-03	2.98	0.66	2.49E-01	2.94	2.45E-01	1.2%	1.8%
20210526	3.58E-03	3.17	1.30	3.51E-02	3.08	3.20E-02	2.7%	9.8%
20210529	1.00E-03	0.68	0.54	1.26E-02	0.60	6.75E-03	12.5%	86.5%
20210619	1.30E-03	7.10	1.06	5.80E-01	7.05	5.78E-01	0.6%	0.3%
20210620	1.64E-03	3.92	1.11	2.90E-01	3.85	2.84E-01	1.9%	2.4%
20210621	4.81E-03	1.50	2.33	7.33E-05	1.33	2.18E-05	11.3%	236.2%

Date	$CoagS_{1.5}$	$GR_{<3}$	GR_{H2SO4}	P1*	$GR_{<3}$ - GR_{HIO3}	P2*	GR contribution	$SP_{1.5-3}$ EF
20210802	1.01E-03	2.11	1.02	2.41E-01	1.73	1.77E-01	17.9%	36.2%
20210827	2.51E-03	0.86	2.25	1.69E-04	0.55	1.40E-06	35.5%	11921.9%
20210929	2.43E-03	1.84	1.09	1.98E-02	1.79	1.77E-02	2.7%	11.8%

Note: P1 represents the survival probability calculated from measured GR; P2 represents the survival probability calculated from measured GR subtracted by GR contributed from HIO_3 concentration solely. Meanings of P1 and P2 in following Tables (Table S3~S7) are identical with them in this table.

Table S3. The GR contributions and SP enhancements of HIO_3 to particles in the size range between 1.5 nm to 3 nm on each NPF event days in Beijing based on APT-y.

Date	$CoagS_{1.5}$	$GR_{1.5-3}$	GR_{H2SO4}	P1	$GR_{1.5-3}$ - GR_{HIO3}	P2	$GR_{1.5-3}$ contributions	$SP_{1.5-3}$ EF
20190818	2.21E-03	1.80	1.38	2.61E-02	1.76	2.42E-02	2.0%	7.8%
20190823	3.13E-03	4.66	1.63	1.36E-01	4.64	1.35E-01	0.4%	0.7%
20190830	1.91E-03	8.40	1.26	5.09E-01	8.36	5.07E-01	0.5%	0.4%
20210525	1.40E-03	3.30	0.66	2.85E-01	3.26	2.81E-01	1.1%	1.4%
20210526	3.58E-03	5.13	1.30	1.26E-01	5.04	1.22E-01	1.7%	3.6%
20210529	1.00E-03	0.70	0.54	1.45E-02	0.62	8.08E-03	12.0%	78.9%
20210619	1.30E-03	8.38	1.06	6.30E-01	8.33	6.29E-01	0.5%	0.2%
20210620	1.64E-03	4.64	1.11	3.51E-01	4.56	3.46E-01	1.6%	1.7%
20210621	4.81E-03	1.92	2.33	6.07E-04	1.76	2.97E-04	8.8%	104.1%
20210802	1.01E-03	4.30	1.02	4.98E-01	3.92	4.65E-01	8.8%	6.9%
20210827	2.51E-03	1.11	2.25	1.23E-03	0.81	9.85E-05	27.4%	1151.9%
20210929	2.43E-03	2.87	1.09	8.12E-02	2.82	7.76E-02	1.8%	4.7%

Table S4. The GR contributions and SP enhancements of HIO_3 to particles in the size range between 1.5 nm to 3 nm on each NPF event days in Beijing based on MOD.

Date	$CoagS_{1.5}$	$GR_{1.5\text{-}3}$	GR_{H2SO4}	P1	$GR_{1.5\text{-}3}$ - GR_{HIO3}	P2	$GR_{1.5\text{-}3}$ contributions	$SP_{1.5\text{-}3}$ EF
20190830	1.91E-03	3.64	1.26	2.10E-01	3.59	2.06E-01	1.2%	2.0%
20210525	1.40E-03	0.84	0.66	7.30E-03	0.80	5.83E-03	4.4%	25.2%
20210526	3.58E-03	2.22	1.30	8.45E-03	2.14	6.98E-03	3.9%	21.1%
20210529	1.00E-03	0.90	0.54	3.73E-02	0.82	2.65E-02	9.4%	40.5%
20210619	1.30E-03	1.50	1.06	7.64E-02	1.46	7.10E-02	2.8%	7.7%
20210620	1.64E-03	1.00	1.11	7.78E-03	0.93	5.29E-03	7.4%	47.1%
20210621	4.81E-03	1.93	2.33	6.14E-04	1.76	3.01E-04	8.8%	103.7%
20210802	1.01E-03	1.40	1.02	1.18E-01	1.03	5.40E-02	26.8%	118.8%
20210827	2.51E-03	2.20	2.25	3.40E-02	1.90	1.97E-02	13.8%	72.1%

Table S5. The GR contributions and SP enhancements of HIO_3 to particles in the size range between 3 nm to 7 nm on each NPF event days in Beijing based on APT-x.

Date	$CoagS_3$	$GR_{3\text{-}7}$	P1	$GR_{3\text{-}7}$ - GR_{HIO3}	P2	$GR_{3\text{-}7}$ contributions	$SP_{3\text{-}7}$ EF
20190818	7.40E-04	2.62	0.142	2.58	0.138	1.4%	2.8%
20190823	8.50E-04	5.83	0.365	5.79	0.363	0.6%	0.6%
20190828	2.39E-04	5.54	0.743	5.45	0.739	1.6%	0.5%
20190830	5.42E-04	5.87	0.529	5.82	0.526	1.0%	0.6%
20190914	7.19E-04	2.34	0.121	2.27	0.112	3.2%	7.3%
20190918	2.96E-04	2.15	0.387	2.11	0.380	1.7%	1.6%
20190924	5.89E-04	7.64	0.587	7.60	0.585	0.6%	0.3%
20200524	3.56E-04	3.61	0.506	3.39	0.485	5.9%	4.4%
20200526	2.92E-04	4.79	0.656	4.68	0.650	2.3%	1.0%
20200527	3.17E-04	15.24	0.866	15.03	0.864	1.4%	0.2%
20200614	1.48E-04	2.03	0.606	1.93	0.589	5.2%	2.8%

Date	$CoagS_3$	GR_{3-7}	P1	GR_{3-7} - GR_{HIO3}	P2	GR_{3-7} contributions	SP_{3-7} EF
20200902	1.27E-03	2.96	0.051	2.89	0.048	2.3%	7.3%
20200903	1.62E-05	9.97	0.989	9.87	0.989	1.0%	0.1%
20210525	3.87E-04	4.60	0.559	4.57	0.557	0.7%	0.4%
20210526	9.44E-04	10.91	0.550	10.82	0.548	0.9%	0.5%
20210529	3.50E-04	0.55	0.013	0.46	0.006	16.3%	133.6%
20210619	3.90E-04	5.14	0.592	5.09	0.589	1.0%	0.5%
20210620	5.04E-04	7.42	0.626	7.36	0.623	0.8%	0.4%
20210621	1.35E-03	3.68	0.080	3.50	0.070	5.1%	14.6%
20210622	9.37E-04	5.82	0.329	5.66	0.319	2.8%	3.2%
20210802	3.30E-04	5.00	0.634	4.74	0.618	5.4%	2.6%
20210827	7.29E-04	4.57	0.332	4.29	0.309	6.2%	7.5%
20210929	6.02E-04	10.17	0.665	10.11	0.663	0.6%	0.3%

Table S6. The GR contributions and SP enhancements of HIO_3 to particles in the size range between 3 nm to 7 nm on each NPF event days in Beijing based on APT-y.

Date	$CoagS_3$	GR_{3-7}	P1	GR_{3-7} - GR_{HIO3}	P2	GR_{3-7} contributions	SP_{3-7} EF
20190818	7.40E-04	2.66	0.147	2.63	0.143	1.4%	2.7%
20190823	8.50E-04	5.87	0.368	5.84	0.366	0.6%	0.6%
20190828	2.39E-04	5.68	0.748	5.59	0.745	1.6%	0.5%
20190830	5.42E-04	5.91	0.531	5.85	0.527	1.0%	0.6%
20190914	7.19E-04	3.41	0.233	3.33	0.226	2.2%	3.4%
20190918	2.96E-04	2.18	0.392	2.15	0.386	1.7%	1.6%
20190924	5.89E-04	8.69	0.626	8.65	0.625	0.5%	0.2%
20200524	3.56E-04	3.81	0.525	3.60	0.505	5.6%	3.9%
20200526	2.92E-04	4.97	0.666	4.86	0.660	2.2%	0.9%
20200527	3.17E-04	16.19	0.874	15.98	0.872	1.3%	0.2%

Date	$CoagS_3$	GR_{3-7}	P1	GR_{3-7} - GR_{HIO3}	P2	GR_{3-7} contributions	SP_{3-7} EF
20200614	1.48E-04	2.06	0.609	1.95	0.593	5.2%	2.8%
20200902	1.27E-03	3.27	0.068	3.20	0.064	2.1%	6.0%
20200903	1.62E-05	13.44	0.992	13.35	0.992	0.7%	0.1%
20210525	3.87E-04	5.75	0.628	5.72	0.627	0.6%	0.3%
20210526	9.44E-04	14.11	0.630	14.02	0.628	0.7%	0.3%
20210529	3.50E-04	0.89	0.066	0.80	0.049	10.2%	36.1%
20210619	3.90E-04	5.19	0.595	5.14	0.592	1.0%	0.5%
20210620	5.04E-04	7.45	0.627	7.39	0.625	0.8%	0.4%
20210621	1.35E-03	3.78	0.085	3.59	0.075	5.0%	13.8%
20210622	9.37E-04	5.98	0.339	5.82	0.329	2.7%	3.0%
20210802	3.30E-04	5.13	0.642	4.86	0.626	5.2%	2.5%
20210827	7.29E-04	4.86	0.355	4.57	0.333	5.8%	6.6%
20210929	6.02E-04	11.06	0.687	11.00	0.685	0.6%	0.2%

210

Table S7. The GR contributions and SP enhancements of HIO_3 to particles in the size range between 3 nm to 7 nm on each NPF event days in Beijing based on MOD.

Date	$CoagS_3$	GR_{3-7}	P1	GR_{3-7} - GR_{HIO3}	P2	GR_{3-7} contributions	SP_{3-7} EF
20190818	7.40E-04	2.75	0.156	2.71	0.152	1.3%	2.5%
20190823	8.50E-04	3.55	0.192	3.52	0.189	1.0%	1.6%
20190828	2.39E-04	3.56	0.630	3.47	0.622	2.5%	1.2%
20190830	5.42E-04	3.49	0.342	3.43	0.336	1.6%	1.8%
20190914	7.19E-04	2.99	0.190	2.91	0.182	2.5%	4.4%
20190918	2.96E-04	4.51	0.636	4.47	0.633	0.8%	0.4%
20190924	5.89E-04	3.13	0.273	3.09	0.268	1.3%	1.8%
20200524	3.56E-04	2.41	0.361	2.20	0.327	8.9%	10.4%
20200526	2.92E-04	2.95	0.505	2.84	0.491	3.7%	2.7%

Date	$CoagS_3$	GR_{3-7}	P1	GR_{3-7} - GR_{HIO3}	P2	GR_{3-7} contributions	SP_{3-7} EF
20200527	3.17E-04	1.13	0.145	0.92	0.092	19.1%	57.6%
20200614	1.48E-04	2.46	0.660	2.35	0.648	4.3%	1.9%
20200902	1.27E-03	3.48	0.080	3.41	0.076	2.0%	5.2%
20200903	1.62E-05	4.32	0.974	4.22	0.974	2.3%	0.1%
20210525	3.87E-04	1.69	0.205	1.66	0.199	1.9%	3.1%
20210526	9.44E-04	4.43	0.229	4.33	0.222	2.1%	3.2%
20210529	3.50E-04	2.06	0.310	1.97	0.294	4.4%	5.5%
20210619	3.90E-04	3.90	0.501	3.84	0.496	1.3%	0.9%
20210620	5.04E-04	1.83	0.149	1.77	0.140	3.1%	6.2%
20210621	1.35E-03	1.93	0.008	1.74	0.005	9.7%	68.5%
20210622	9.37E-04	2.54	0.078	2.38	0.066	6.3%	18.7%
20210802	3.30E-04	1.82	0.286	1.55	0.230	14.8%	24.3%
20210827	7.29E-04	2.20	0.102	1.92	0.073	12.8%	39.9%
20210929	6.02E-04	1.89	0.111	1.83	0.103	3.3%	7.8%

Table S8. NPF event day identified at SORPES and the contribution to growth of two acids in different size ranges and the ratio in each case.

DATE	$GR_{1.5-3}$(IA)	$GR_{1.5-3}$(SA)	$Ratio_{1.5-3}$
2019-06-17	0.15	2.39	6.1%
2019-06-21	0.15	2.14	6.8%
2019-07-03	0.39	2.65	14.6%
2019-07-11	0.26	2.97	8.6%
2019-07-13	0.16	2.06	7.5%
2019-07-19	0.13	1.33	10.0%
2019-07-30	0.09	2.83	3.3%
2019-08-09	0.05	3.50	1.4%
2019-08-16	0.19	2.45	7.9%
2019-08-17	0.09	2.93	3.2%
2019-08-18	0.40	2.80	14.5%
2019-08-27	0.13	1.05	12.8%
2019-10-21	0.09	1.02	8.4%
2019-10-23	0.28	2.19	12.6%

DATE	$GR_{1.5\text{-}3}$(IA)	$GR_{1.5\text{-}3}$(SA)	$Ratio_{1.5\text{-}3}$
2019-10-26	0.14	1.28	10.7%
2019-10-31	0.04	2.01	2.1%
2019-11-01	0.11	2.75	3.9%
2019-11-05	0.06	2.06	2.9%
2019-11-10	0.04	0.91	4.0%
2019-11-11	0.03	1.26	2.4%
2019-11-14	0.03	0.89	2.8%
2019-11-19	0.02	1.01	2.4%
2019-11-20	0.08	1.64	4.8%

Table S9. NPF event day identified at SORPES and the contribution to particle survival probability of two acids in different size ranges and the enhancement of survival probability in each case.

DATE	$SP_{1.5\text{-}3}$(SA)	$SP_{1.5\text{-}3}$(SA+IA)	$SP_{1.5\text{-}3}$EF
2019-06-17	-	-	-
2019-06-21	1.13E-03	1.75E-03	54.3%
2019-07-03	4.16E-03	8.34E-03	100.7%
2019-07-11	7.26E-03	1.07E-02	47.6%
2019-07-13	2.16E-03	3.32E-03	53.8%
2019-07-19	1.40E-02	2.07E-02	47.5%
2019-07-30	9.56E-03	1.11E-02	15.9%
2019-08-09	8.80E-02	9.10E-02	3.4%
2019-08-16	3.15E-03	4.80E-03	52.7%
2019-08-17	5.84E-04	7.37E-04	26.3%
2019-08-18	2.27E-02	3.66E-02	61.4%
2019-08-27	3.24E-03	6.20E-03	97.7%
2019-10-21	-	-	-
2019-10-23	-	-	-
2019-10-26	6.06E-04	1.24E-03	104.9%
2019-10-31	1.10E-05	1.39E-05	25.8%
2019-11-01	9.15E-03	1.09E-02	19.1%
2019-11-05	1.32E-04	1.70E-04	29.1%
2019-11-10	-	-	-
2019-11-11	-	-	-
2019-11-14	-	-	-
2019-11-19	-	-	-
2019-11-20	-	-	-

References

Kulmala, M., Kerminen, V. M., Petaja, T., Ding, A. J., and Wang, L.: Atmospheric gas-to-particle conversion: why NPF events are observed in megacities?, Faraday Discuss, 200, 271-288, 10.1039/c6fd00257a, 2017.

Kulmala, M., Petaja, T., Nieminen, T., Sipila, M., Manninen, H. E., Lehtipalo, K., Dal Maso, M., Aalto, P. P., Junninen, H., Paasonen, P., Riipinen, I., Lehtinen, K. E., Laaksonen, A., and Kerminen, V. M.: Measurement of the nucleation of atmospheric aerosol particles, Nat Protoc, 7, 1651-1667, 10.1038/nprot.2012.091, 2012.

Manninen, H. E., Mirme, S., Mirme, A., Petäjä, T., and Kulmala, M.: How to reliably detect molecular clusters and nucleation mode particles with Neutral cluster and Air Ion Spectrometer (NAIS), Atmos. Meas. Tech., 9, 3577-3605, 10.5194/amt-9-3577-2016, 2016.

Stein, A. F., Draxler, R. R., Rolph, G. D., Stunder, B. J. B., Cohen, M. D., and Ngan, F.: NOAA's HYSPLIT Atmospheric Transport and Dispersion Modeling System, Bulletin of the American Meteorological Society, 96, 2059-2077, https://doi.org/10.1175/BAMS-D-14-00110.1, 2015.

Stolzenburg, D., Cai, R., Blichner, S. M., Kontkanen, J., Zhou, P., Makkonen, R., Kerminen, V.-M., Kulmala, M., Riipinen, I., and Kangasluoma, J.: Atmospheric nanoparticle growth, Reviews of Modern Physics, 95, 045002, 10.1103/RevModPhys.95.045002, 2023.

Wang, Y. Q.: MeteoInfo: GIS software for meteorological data visualization and analysis, Meteorological Applications, 21, 360-368, 10.1002/met.1345, 2014.